

Mapping the cosmic expansion history from LIGO-Virgo-KAGRA in synergy with DESI and SPHEREx

Cristina Cigarrán Díaz¹, Suvodip Mukherjee^{1,2,3} † ‡ 

¹ *Gravitation Astroparticle Physics Amsterdam (GRAPPA), Anton Pannekoek Institute for Astronomy and Institute for Physics, University of Amsterdam, Science Park 904, 1090 GL Amsterdam, The Netherlands*

² *Institute Lorentz, Leiden University, PO Box 9506, Leiden 2300 RA, The Netherlands*

³ *Delta Institute for Theoretical Physics, Science Park 904, 1090 GL Amsterdam, The Netherlands*

28 July 2021

ABSTRACT

The measurement of the expansion history of the Universe from the redshift unknown gravitational wave (GW) sources (dark GW sources) detectable from the network of LIGO-Virgo-KAGRA (LVK) detectors depends on the synergy with the galaxy surveys having accurate redshift measurements over a broad redshift range, large sky coverage, and detectability of fainter galaxies. In this work, we explore the possible synergy of the LVK with the spectroscopic galaxy surveys such as DESI and SPHEREx to measure the cosmological parameters which are related to the cosmic expansion history and the GW bias parameters. We show that by using the three-dimensional spatial cross-correlation between the dark GW sources and the spectroscopic galaxy samples, we can measure the value of Hubble constant with about 2% and 1.5% precision from LVK+DESI and LVK+SPHEREx respectively from the five years of observation with 50% duty-cycle for the GW merger rates driven by the star formation history. Similarly, the dark energy equation of state can be measured with about 10% and 8% precision from LVK+DESI and LVK+SPHEREx respectively. We find that due to the larger sky coverage of SPHEREx than DESI, the performance in constraining the cosmological parameters is better from the former than the latter. By combining Euclid along with DESI, and SPHEREx a marginal gain in the measurability of the cosmological parameters is possible from the sources at high redshift ($z \geq 0.9$).

Key words: gravitational waves, black hole mergers, cosmology: miscellaneous

1 INTRODUCTION

Mapping the cosmic expansion history at different redshift provides a direct way to unveil the constituents of the Universe. Gravitational waves (GWs) provide a robust way to achieve this with the aid of coalescing binary compact objects such as binary neutron stars (BNSs), neutron star black holes (NSBHs), and binary black holes (BBHs) systems which are *standard sirens* if the emission of GWs from these systems can be completely predictable by the General Theory of Relativity and redshift to these sources can be measured independently, as shown for the first time in the seminal work by Schutz (1986). Though the direct measurement of the source redshift using the GW signal is not possible due to the mass-redshift degeneracy, several techniques are proposed such as the spectroscopic measurement of the redshift of the host galaxy from electromagnetic counterpart (Schutz 1986; Holz & Hughes 2005; Dalal et al. 2006; MacLeod & Hogan 2008; Nissanke et al. 2010; Schutz 2011; Chen et al. 2018; Feeney et al. 2019), tidal-deformability of neutron star (Messenger &

Read 2012), known mass-scale (Farr et al. 2019; Mastrogiovanni et al. 2021a), statistical host identification (Del Pozzo 2012; Arabsalmani et al. 2013; Chen et al. 2018; Nair et al. 2018; Gray et al. 2020; Fishbach et al. 2019; Abbott et al. 2019a; Soares-Santos et al. 2019; Abbott et al. 2020d), and exploring the spatial clustering-scale between the GW sources and galaxies (Oguri 2016; Mukherjee & Wandelt 2018; Mukherjee et al. 2020c, 2021b; Bera et al. 2020; Mukherjee et al. 2021c) to independently infer the redshift of the GW sources. With the aid of these techniques, it is expected that using the plethora of GW sources which are detectable in the coming years from the current generation GW detectors such as Laser Interferometer Gravitational-wave Observatory (LIGO) (Aasi et al. 2015a; Abbott et al. 2016b), Virgo (Acernese et al. 2014, 2019), Kamioka Gravitational Wave Detector (KAGRA) (Akutsu et al. 2019a, 2020), LIGO-India (Unnikrishnan 2013)¹, we can achieve accurate and precise measurement of the expansion history, if detector systematics can be mitigated successfully (Sun et al. 2020; Bhattacharjee et al. 2020; Vitale et al. 2021).

† Corresponding author (s.mukherjee@uva.nl)

‡ The author list is in the alphabetical order.

¹ LIGO-India, Proposal of the Consortium for Indian Initiative in Gravitational-wave Observations (IndIGO).

Such an independent measurement is going to play a vital role in resolving the tension in the value of the current expansion rate of the Universe known as the Hubble constant between the late Universe probes (Riess et al. 2019; Riess 2019; Wong et al. 2020; Freedman et al. 2019, 2020; Soltis et al. 2021) and the early Universe probes (Spergel et al. 2003, 2007; Komatsu et al. 2011; Planck collaboration 2014; Ade et al. 2016; Alam et al. 2017b; Aghanim et al. 2018; Alam et al. 2021; Aiola et al. 2020) and will also be capable to shed light on the nature of dark matter and dark energy which constitutes about 95% of the energy budget of the Universe, as indicated by the measurements from electromagnetic probes such as supernovae (Perlmutter et al. 1999; Reid et al. 2009; Riess et al. 2019), cosmic microwave background (Spergel et al. 2003, 2007; Komatsu et al. 2011; Planck collaboration 2014; Ade et al. 2016; Aghanim et al. 2018; Aiola et al. 2020), and baryon acoustic oscillation (Eisenstein & Hu 1998, 1997; Dawson et al. 2013; Alam et al. 2017b, 2021).

Since the discovery of GW (Abbott et al. 2016c) by the LIGO-Virgo Scientific Collaboration and followed by the detection of about 50 GW sources until the first half of the third observation run (Abbott et al. 2019b, 2021), we have seen one BNS event GW170817 (Abbott et al. 2017a) with electromagnetic counterpart (Kasliwal et al. 2017; Abbott et al. 2017b), which enabled the first measurement of Hubble constant $H_0 = 70_{-8}^{+12}$ km/s/Mpc. A revised value after incorporating with a different peculiar velocity correction scheme is obtained by Howlett & Davis (2020); Mukherjee et al. (2021d); Nicolaou et al. (2020). For one of the BBH event GW190521 (Abbott et al. 2020b) detected by the LIGO-Virgo detectors, there was a plausible electromagnetic counterpart detected by the Zwicky transient facility (ZTF) (Graham et al. 2020), which provided only a weak measurement of the value of Hubble constant $H_0 = 62.2_{-19.7}^{+29.5}$ km/s/Mpc (Mukherjee et al. 2020a) for the SEOBNRv4PHM waveform². Measurement of the value of Hubble constant using GW190521 is also performed by several other independent studies (Chen et al. 2020; Gayathri et al. 2021; Mastrogianni et al. 2021b). The sources which did not show any electromagnetic counterpart (also called dark sirens), were used to measure the value of the Hubble constant by the statistical host identification technique (Gray et al. 2020) using the sources detected in the first two observation runs (O1+O2) (Abbott et al. 2019a) using the GLADE catalog (Dálya et al. 2018). More recently, using the GW events from O1+O2+O3a, a value of $H_0 = 67.3_{-17.9}^{+27.6}$ km/s/Mpc is obtained by Finke et al. (2021).

The discovery made by the LIGO-Virgo detectors agrees with our current understanding, that we only expect electromagnetic counterparts from GW sources such as BNS and NS-BH systems (Foucart et al. 2018). For BBHs, unless there is a presence of baryonic matter (McKernan et al. 2019; Yang et al. 2019; Tagawa et al. 2021), electromagnetic counterparts are not expected in standard scenarios. However, the number of BBHs is expected to be more in number as it can be detected up to a larger luminosity distance and hence can encompass more cosmic volume. So to use these large detectable BBHs as standard sirens to study cosmology, robust

techniques are required to make an accurate and precise measurement of the redshift is required.

One such method which is free from any astrophysical assumption about the GW source property or population is through the exploration of the three-dimensional spatial clustering between GW sources and galaxies by using the three-dimensional cross-correlation technique (Mukherjee & Wandelt 2018; Mukherjee et al. 2020c, 2021b). However, the success of this method depends on the availability of the galaxy surveys with accurate redshift measurement in the overlapping sky area of the GW sources and also up to a deeper high redshift and have access to fainter galaxies. For a single galaxy survey to satisfy all the criteria is difficult to achieve. But by combining multiple galaxy surveys, one can reach the requirements to apply the cross-correlation technique to dark standard sirens. In this work, we explore the synergy between the upcoming spectroscopic galaxy surveys such Dark Energy Spectroscopic Instrument (DESI) (Aghamousa et al. 2016) and Spectro-Photometer for the History of the Universe, Epoch of Reionization, and Ices Explorer (SPHEREx) (Doré et al. 2014) with the GW sources which are detectable from the network of four GW detectors (LIGO-Livingston, LIGO-Hanford, Virgo, and KAGRA), hereafter LVK (Abbott et al. 2018), for different scenarios of GW merger rates motivated from the Madau & Dickinson (2014) star formation rate. We show the expected overlap between GW merger rates and galaxy surveys for different time-delay scenarios and apply the cross-correlation technique on the simulated GW sources for the network of four detectors using the publicly available package Bilby (Ashton et al. 2019) with the mock DESI and SPHEREx galaxy samples. This paper is organized as follows, in Sec. 2, we discuss the GW source population and merger rates for different time-delay scenarios. In Sec. 3, we set the detail formalism for the cross-correlation method between GW sources and galaxies. In Sec. 4 and Sec. 5 we will discuss the requirements for exploring the synergy between galaxy surveys and dark standard sirens and brief descriptions of the upcoming galaxy surveys respectively. In section 6 we discuss the simulated mock GW and galaxy catalog considered in this analysis and Sec. 7 we make forecasts of estimating the cosmological parameters from LVK+DESI and LVK+SPHEREx combinations with the five years of LVK observation run in its design sensitivity with 50% duty cycle. We conclude in Sec. 8 with the future scope of this study.

2 GW SOURCE PROPERTIES

2.1 GW mass distribution

The GWTC-2 (Abbott et al. 2021) catalog includes the first half of the third observing run, O3a (Abbott et al. 2021), and the first and second observing run, O1 and O2 (Abbott et al. 2019b), of the Advanced LIGO (Aasi et al. 2015b) and Advanced Virgo (Acernese et al. 2014) gravitational wave detectors. The GWTC-2 includes 44 new BBH events over GWTC-1 and thus allows for the study of the properties of the BBHs population, (Abbott et al. 2020a). In Abbott et al. (2020a), several models are proposed to study the mass distribution of GW events from BBHs such as the Truncated model, Power-law + Peak model, Broken power-law, and

² $H_0 = 50.4_{-19.5}^{+28.1}$ km/s/Mpc for the NRSur7dq4 waveform, and $H_0 = 43.1_{-11.4}^{+24.6}$ km/s/Mpc for the IMRPhenomPv3HM waveform.

Multi peak model. The Bayes factor estimation from GWTC-2 indicates a better fit for the Power-law + Peak model over the other models (Abbott et al. 2021). However, we still are at an early stage to draw any conclusion on the mass distribution of the binary black holes and compare with the possible formation scenarios (Coleman Miller & Hamilton 2002; Gultekin et al. 2004; Antonini & Rasio 2016; Rodriguez et al. 2019).

2.2 GW merger rate models

With the observation of the BBH merger GW150914, (Abbott et al. 2016d), we learned that BBHs indeed merge within the age of the Universe at a detectable rate. Astrophysical black holes (ABHs) and other astrophysical compact objects are produced from the death of stars and are therefore expected that the merger rate of the astrophysical compact objects is going to be related to the star formation rate. However, the time delay t_d^{eff} between the formation and merger of compact objects is still uncertain, it may range between a few 100 Myr to around the age of the Universe (O’Shaughnessy et al. 2010; Banerjee et al. 2010; Dominik et al. 2012; Dominik et al. 2015; Mandel & de Mink 2016; Lamberts et al. 2016; Cao et al. 2018; Elbert et al. 2018; Eldridge et al. 2019; du Buisson et al. 2020; Santoliquido et al. 2021).

The GW merger rate model we consider in this analysis is motivated by the star formation rate model well described by the Madau & Dickinson (2014) relation

$$R_{SFR}(z) = 0.015 \frac{(1+z)^{2.7}}{1 + \left(\frac{1+z}{2.9}\right)^{5.6}} M_{\odot} \text{ Mpc}^{-3} \text{ yr}^{-1}. \quad (1)$$

This SFR model is based on galaxy surveys having rest-frame FUV (far ultra-violet) and FIR (far infrared) measurements. This rate peaks around redshift of a few, $z \sim 2$ (Madau & Dickinson 2014). The GW merger rate can then be written as

$$\mathcal{R}_{GW}^{ABH}(z_m) = \mathcal{N} \int_{z_m}^{\infty} dz \frac{dt_f}{dz} P(t_d^{eff}) R_{SFR}(z), \quad (2)$$

where \mathcal{N} is the normalization such that $\mathcal{R}_{GW}^{ABH}(z=0) = 25 \text{ Gpc}^{-3} \text{ yr}^{-1}$ so it is in agreement with observations from GWTC-2, (Abbott et al. 2020c), and t_d^{eff} is the effective time-delay parameter. $R_{SFR}(z)$ is the star formation rate in Eq. 1. The effective delay time parameter t_d^{eff} probability distribution function is not yet known from observation and thus needs to be modelled. We consider a power-law model for the delay time probability distribution $P(t_d^{eff})$ in our analysis (Mukherjee & Silk 2021; Mukherjee et al. 2021a).

$$P(t_d^{eff}) = 1/t_d^{eff}, \quad t_d^{eff} > t_d^{min}, \quad (3)$$

where t_d^{min} is the minimum value of the time delay. We show in Fig. 1 the GW merger rates for different values of the time-delay parameter t_d^{eff} . The longer time delay causes more shift in the peak of the GW merger rate to a lower redshift than the star formation peak $z \sim 2$. As a result, if the value of the time delay is larger than a few Gyrs, then most of the GW mergers will be happening at a lower redshift and the corresponding galaxy survey needs to have a window function overlapping with the merger rate of the GW sources. We discuss this in further detail in the later section of the paper.

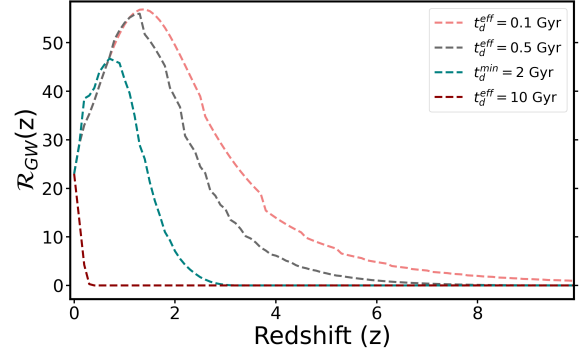


Figure 1. Merger rate of the GW sources for power-law time-delay models, for different values of t_d^{min} (in Gyr). The merger rate is higher for higher redshifts when the value of the time delay is small, while if the value of the time delay is larger the merger rate does not reach such high values at higher redshifts. Furthermore, we can see how the peak of the distribution moves to lower redshifts as we consider higher time delay values.

3 BASIC FORMALISM OF CROSS-CORRELATION BETWEEN GW SOURCES AND GALAXIES

The formalism behind the three-dimensional cross-correlation technique is formulated by Mukherjee et al. (2021b,c). The exploration of the spatial clustering between the GW sources and galaxies can be useful to measure the clustering redshift (Newman 2008; Menard et al. 2013; Schmidt et al. 2013) of the GW sources. We can write the galaxy density field as

$$\delta_g(\mathbf{r}) = \frac{n_g(\mathbf{r})}{\bar{n}_g} - 1, \quad (4)$$

where $n_g(\mathbf{r})$ is the number density of galaxies at a position \mathbf{r} and \bar{n}_g is the mean number density of galaxies. We can relate the spatial distribution of galaxies with the underlying dark matter distribution in the Fourier space $\delta_m(\mathbf{k})$ as

$$\delta_g(\mathbf{k}, z) = b_g(k, z) \delta_m(\mathbf{k}, z), \quad (5)$$

where $b_g(k, z)$ is the galaxy bias parameter which can be both scale and redshift dependent.

Along with the Hubble flow, galaxies also have intrinsic peculiar velocities that will displace them along the line of sight in redshift space and these displacements causes redshift-space distortions (RSD) and its signature gets imprinted in the clustering of galaxies in redshift space. The amplitude of distortions on large scales gives a measure of the linear RSD parameter $\beta_g \equiv f/b_g(k, z)$, which defined in terms of $f \equiv d \ln D/d \ln a$, with D being the growth function, and $\mu_{\hat{k}} = \cos \hat{n} \cdot \hat{k}$ is the angle between the line of sight and the Fourier mode \hat{k} (Hamilton 1998; Kaiser 1987). The growth factor D is defined as $D = \frac{H(z)}{H_0} \int_z^{\infty} \frac{dz'(1+z')}{H(z')^3} \left[\int_0^{\infty} \frac{dz''(1+z'')}{H(z'')^3} \right] - 1$, and it measures the growth of the cosmological perturbations with redshift. The galaxy density field in redshift space $\delta_g^s(\mathbf{k}, z)$ can be written in terms of the physical space density field $\delta_m^r(\mathbf{k}, z)$ by including the effect from RSD as

$$\delta_g^s(\mathbf{k}, z) = b_g(k, z) (1 + \beta_g \mu_{\hat{k}}) \delta_m^r(\mathbf{k}, z). \quad (6)$$

GW events from astrophysical sources will take place in galaxies and will therefore follow the spatial distribution of galaxies with a bias parameter $b_{GW}(k, z)$ - the value of this

parameter is different to the galaxy bias parameter $b_g(k, z)$. We can then define the gravitational wave density field in real space as

$$\delta_{GW}^r(\mathbf{k}, z) = b_{GW}(k, z)\delta_m^r(\mathbf{k}, z), \quad (7)$$

where $b_{GW}(k, z)$ is the gravitational wave bias parameter which measures how GW sources trace the large scale structure of the Universe (Mukherjee & Silk 2019; Mukherjee et al. 2021b). There are also other studies to explore the GW bias parameter (Scelfo et al. 2018; Calore et al. 2020; Vijaykumar et al. 2020; Scelfo et al. 2020).

$$\left\langle \left(\begin{array}{c} \delta_g^s(\mathbf{k}, z) \\ \delta_{GW}^s(\mathbf{k}, z) \end{array} \right) \left(\delta_g^s(\mathbf{k}', z) \delta_{GW}^r(\mathbf{k}', z) \right) \right\rangle = \left(\begin{array}{cc} P_{gg}^{ss}(\mathbf{k}, z)\delta_D(\mathbf{k}-\mathbf{k}') + \bar{n}_g(z)^{-1} & P_g^{sr}(\mathbf{k}, z)\delta_D(\mathbf{k}-\mathbf{k}') \\ P_g^{sr}(\mathbf{k}, z)\delta_D(\mathbf{k}-\mathbf{k}') & P_{GW}^{rr}(\mathbf{k}, z)\delta_D(\mathbf{k}-\mathbf{k}') + \bar{n}_{GW}(z)^{-1} \end{array} \right),$$

where $P_{xy}^{ij}(\mathbf{k}, z)$ is the three dimensional power spectrum at redshift z associated with clustering between two tracers ($\{x, y\} \in \{g, GW\}$) in redshift space or real space ($\{ij\} \in \{s, r\}$), $\delta_D(\mathbf{k}-\mathbf{k}')$ is the Dirac delta function and $\bar{n}_x(z)^{-1}$ represents the shot noise contribution, non-zero only for $x = y$. We can express $P_{xy}^{ij}(\mathbf{k}, z)$ in terms of the matter power spectrum $P_m(k, z)$, (Mukherjee et al. 2021b), as

$$P_{gg}^{ss}(\mathbf{k}, z) = b_g^2(k, z)(1 + \beta_g\mu_k^2)P_m(k, z),$$

$$P_g^{sr}(\mathbf{k}, z) = b_g(k, z)b_{GW}(k, z)(1 + \beta_g\mu_k^2)P_m(k, z),$$

$$P_{GW}^{rr}(\mathbf{k}, z) = b_{GW}^2(k, z)P_m(k, z). \quad (8)$$

We are going to use the above formalism to explore the clustering of the GW sources with galaxy surveys with accurate redshift measurement.

4 IMPORTANT FACTORS TO EXPLORE THE SYNERGY BETWEEN GALAXY SURVEYS AND DARK STANDARD SIRENS

The implementation of the cross-correlation between GW sources and galaxies to explore cosmological parameters and also the GW bias parameters depends on several key aspects. We will list below the key aspects which play a crucial role in the implementation of the cross-correlation technique.

Sky localization error: The accuracy and precision of the cross-correlation technique depend on the amount of small-scale (or large values of Fourier modes k) clustering information that can be used. One of the parameters which control the maximum value of Fourier modes k that can be used in the analysis is the sky localization error. The larger angular size of the sky localization error Ω_{GW} leads to a smoothing of the cross-correlation power spectrum for comoving Fourier modes larger than $k_{max}^p(z) \equiv \frac{\sqrt{8 \ln 2}}{\sqrt{\Omega_{GW}(z)d_c(z)}}$ perpendicular to the line of sight, where $d_c(z)$ is the comoving distance at a redshift z (Mukherjee et al. 2021b). As a result, if the value

The clustering in the matter distribution can be statistically described by the correlation function $\xi(r)$ which is related to the power spectrum by Fourier transformation (Peebles & Groth 1975; McClelland & Silk 1977a,b; Davis & Peebles 1977, 1983; Hamilton 1998; Landy & Szalay 1993). The spatial clustering of galaxies and GW can be written in Fourier space in terms of the auto-power spectrum and cross power-spectrum at different values of the redshift as (Mukherjee et al. 2021b)³

of $\sqrt{\Omega_{GW}d_c}$ is large, then k_{max}^p is small which will lead to a suppression in the cross-correlation estimation for values of Fourier modes k larger than k_{max}^p . As a result, GW sources that are nearby and having better sky localization can have a better measurement of the clustering redshift. So to achieve a better sky localization, we need a network of GW detectors (Abbott et al. 2018; Grover et al. 2014; Howell et al. 2018; Chan 2018) with high detector sensitivity.

Luminosity distance uncertainty: The uncertainty on the luminosity distance to the GW sources plays a crucial role in the cross-correlation technique. The presence of luminosity distance uncertainty causes smearing of the correlation function along the line of sight. For the Fourier modes larger than $k_{max}^l \equiv (1+z)/\sigma_{d_l}$, the contribution to the cross-correlation signal gets suppressed for comoving Fourier modes greater than k_{max}^l . As a result, sources with smaller luminosity distance errors are more useful for measuring the cosmological parameters using the cross-correlation technique than the sources having larger luminosity distance errors.

Overlapping sky area between GW sources and galaxy surveys: The implementation of the cross-correlation technique between the GW sources and galaxies requires to have overlapping sky footprints for both these sectors. A network of GW detectors can detect sources from all the sky directions, though with different sensitivities in different directions depending on the position of the detectors. However, for the galaxy surveys, full-sky coverage from a single mission is possible only from space-based detectors, and not from the ground. From the ground (depending on the location of the detector), we can map only a fraction of the sky. However, by combining the data from multiple telescopes, we can enhance the total footprint of the galaxy surveys. So, the implementation of the cross-correlation technique will be best for a full sky-mission or combinations of several missions to cover a large sky fraction.

Accurate redshift estimation of galaxies: For the estimation of the clustering redshift of the GW sources by the cross-correlation technique, the estimated redshift of the galaxies needs to be accurate and precise. So, the best synergy between the GW sources and galaxy surveys can be explored with galaxies having spectroscopic redshift measurements.

³ The notation $\langle \cdot \rangle$ denotes the ensemble average.

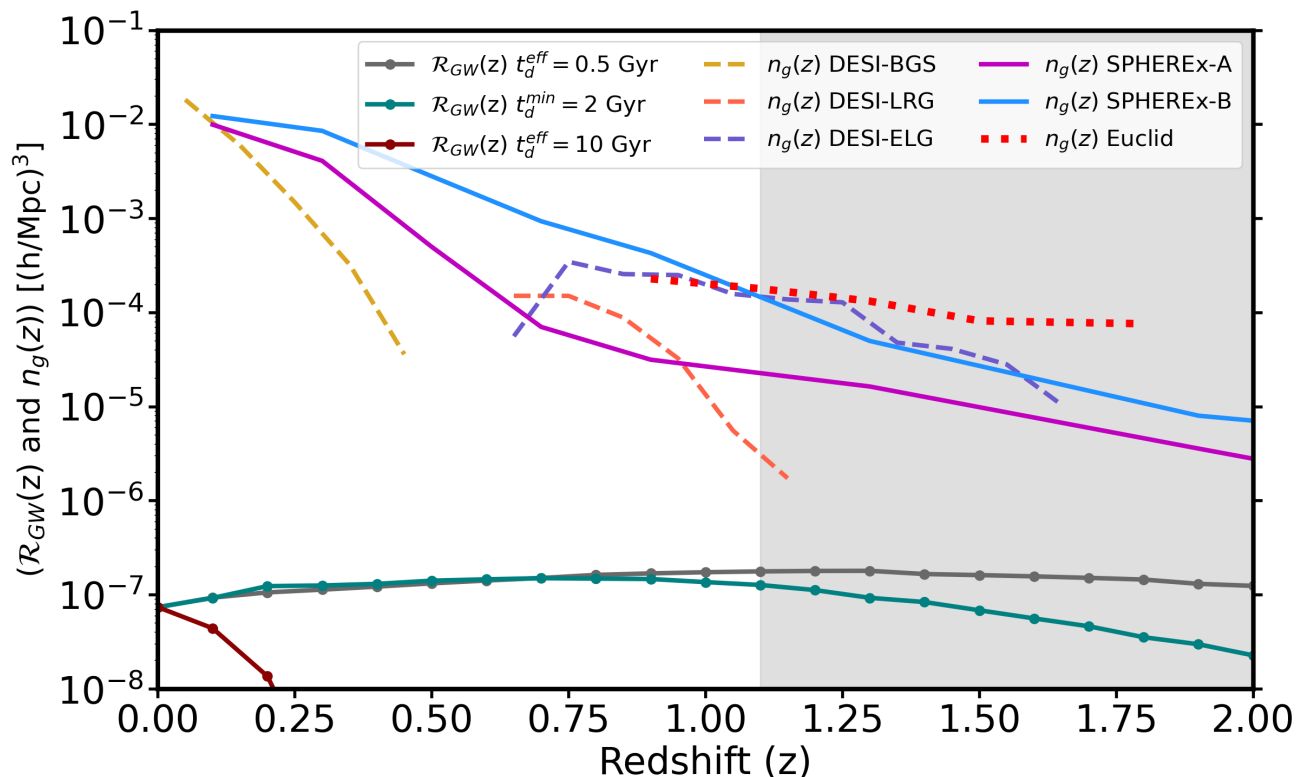


Figure 2. We show the overlap in redshift between the different galaxy surveys along with the possible GW mergers for three different time delay model integrated over one year observation time. The shaded region in grey denotes the redshift for which detection beyond network matched-filtering signal to noise ratio greater than eight is not possible for most of the sources.

The spectroscopic measurement of the galaxy redshift can give us an unbiased redshift estimation and also uncertainty $\sigma_z/(1+z)$ around $\sim 10^{-3}$. For galaxy surveys with photometric redshift measurements, the uncertainty on redshift can be of the order of a few percent ($\geq 2\%$) and may not be completely accurate. So, in this analysis, we will only explore the synergy with the upcoming/ongoing spectroscopic galaxy surveys. The possibility of using the photometric redshift measurements will be explored in a future work where we will include a marginalization over the photometric redshift uncertainty of the galaxies in a Bayesian framework.

Redshift distribution of galaxies: The cross-correlation of the GW sources with galaxy relies on the availability of galaxies samples up to high redshift. Though the presence of host galaxy in the catalog is not required for the application of the cross-correlation technique (Mukherjee & Wandelt 2018; Mukherjee et al. 2021b; Bera et al. 2020), one of the essential quantities in the cross-correlation study is the number-density of the galaxy as a function of redshift ($n_g(z)$). If the number density of the galaxy is large, then the total signal-to-noise ratio (SNR) of the cross-correlation signal increases due to the decrease in the shot-noise contribution. This becomes useful to enhance the accuracy of the estimation of the clustering redshift and also reducing the error on the redshift estimation. So, galaxy surveys with higher galaxy number density are essential to explore cross-correlation with GW sources.

5 ONGOING/UPCOMING SURVEYS OF GW AND GALAXIES WHICH CAN MAKE THE CROSS-CORRELATION STUDY FEASIBLE

In this section, we discuss the ongoing/upcoming detectors in the field of GW and galaxy survey which can play a crucial role to explore the synergy between both these sectors. We show in Fig. 2 the overlap in the redshift for different spectroscopic galaxy surveys with the GW sources with different time-delays. The shaded region in Fig. 2 denotes the redshift range which is inaccessible from the network of LVK detectors.

5.1 Network of GW detectors

A network of GW detectors helps in improving the sky localization error and also reducing the uncertainty in the luminosity distance. As result, the cross-correlation study becomes effective with a network of GW detectors. We consider a network of four GW detectors namely the two LIGO detectors (LIGO-Hanford and LIGO-Livingston) (Aasi et al. 2015b), Virgo (Acernese et al. 2014), and KAGRA (Akutsu et al. 2019b) in their design sensitivity. Currently, LIGO-Hanford, LIGO-Livingston, and Virgo are operational, and from 2022, the KAGRA will likely be operational. We have used five years of observation time with a 50% duty cycle in our analysis. Further improvement in the sky localization error is possible with the operation of a fifth GW detector, LIGO-India (Unnikrishnan 2013). We will not consider

LIGO-India in this work and will defer the study to a future study.

5.2 Spectroscopic galaxy surveys

To be able to perform the cross correlation technique, we need galaxy surveys which satisfies the criteria mentioned in Sec. 4. One of the crucial requirements for the cross-correlation method is to have accurate redshift estimation to galaxies. So, we have explored the possible synergy with the spectroscopic surveys such as DESI (Aghamousa et al. 2016), SPHEREx (Doré et al. 2014), and EUCLID (Laureijs et al. 2011) in this paper. We do not include Roman Telescope (Green et al. 2012; Spergel et al. 2013; Dore et al. 2018a) in this analysis, as the final design still at the stage of preparation. In a future work (Under preparation), we will be explore the synergy between Roman Telescope (Green et al. 2012; Spergel et al. 2013; Dore et al. 2018a) and Vera Rubin Observatory (LSST Science Collaboration et al. 2009) with the LVK detectors.

5.2.1 DESI

DESI (Aghamousa et al. 2016) is a ground-based dark-energy experiment designed to study baryon acoustic oscillations (BAO) and the growth structure through redshift-space distortions with a wide-area galaxy and quasar redshift survey. It will conduct a 5-year survey designed to cover 14,000 deg², which corresponds to a sky fraction $f_{sky} = 0.3$. DESI will survey at $0.4 < z < 3.5$ using luminous red galaxies (LRGs), emission-line galaxies (ELGs), and quasars, to measure the large-scale clustering of the Universe: they will measure LRGs up to $z = 1$, ELGs up to $z = 1.7$ and quasar up to $z = 3.5$. It will also carry out a Bright Galaxy Survey (BGS) of the $z < 0.4$ Universe, which will consist of approximately 10 million galaxies. In total, they will make more than 30 million galaxies and quasars. DESI will use a combination of three telescopes to provide the baseline targeting data. The first of their targets is the Bright Galaxy Sample (BGS), the estimated redshift distribution peaks at $z = 0.2$. As for LRGs, the expected redshift peaks at redshift $z < 0.8$. The ELGs redshift distribution peaks at around $z = 0.8$ and it does not drop to a level where shot noise dominates BAO measurements until $z \approx 1.3$. Lastly, the expected redshift distribution for QSO peaks at around $z \approx 1.6$.

In our work, we are covering the redshift range from $z = 0.1$ to $z = 0.5$. Taking into account the galaxy density distributions in Fig. 2, we can see that there will be an overlap in redshift between our analysis and DESI's LRGs measurements in the higher redshift range of our analysis and with BGS measurements up to around $z = 0.4$.

5.2.2 SPHEREx

SPHEREx (Doré et al. 2014; Dore et al. 2018b) is an all-sky spectroscopy survey satellite designed to probe the origin and density of the Universe. It focuses on the low-redshift Universe and aims to determine the redshifts of hundreds of millions of galaxies. The brightness of the galaxy strongly correlates with the redshift error and thus, they classify galaxies

according to their redshift accuracy. They expect to measure approximately 9 million galaxies with 0.3% accuracy up to $z \approx 0.6$. We can see in Fig. 2 the observed galaxy density for the redshift error $\sigma_z = 0.003(1+z)$ and $\sigma_z = 0.01(1+z)$ respectively shown in magenta (SPHEREx-A) and blue (SPHEREx-B). We restrict to these redshifts bins because high-accuracy redshift measurements are necessary to allow for clustering measurement and thus apply the cross-correlation technique.

SPHEREx derives the photometric redshift of galaxies extracting the flux from simulated images based of galaxy spectral density energy distribution (SEDs) from real data and then fitting template SEDs to the observations. This gives the redshift probability distribution function (PDF), $P(z)$, from which they obtain the best redshift estimate $\bar{z} = \frac{\sum_i z_i P(z_i)}{\sum_i P(z_i)}$ and the error on the estimate $\sigma_{\bar{z}} = \sqrt{\frac{\sum_i (z_i - \bar{z})^2 P(z_i)}{\sum_i P(z_i)}}$ (Doré et al. 2014).

5.2.3 Euclid

Euclid (Laureijs et al. 2011; Blanchard et al. 2020) will cover 15,000 deg² of the northern and southern extragalactic sky and will measure spectroscopic redshifts of 30 million galaxies in the redshift range $0.9 < z < 1.8$ with an spectroscopic redshift error of $0.001(1+z)$. The expected number density of galaxies, i.e of observed H α emitters, for each redshift bin in the given redshift range is of the order of 10^{-4} ($h^3\text{Mpc}^{-3}$), as we can see in Fig. 2. So, the overlap between the Euclid galaxy samples and the GW sources will be only at high redshift $0.9 < z < 1.1$. For these sources, the luminosity distance error and sky localization error will be large for LVK network of detectors. As a result, the cross-correlation technique will not be effective. However, it is important to include Euclid in the combined catalog of galaxy surveys, to allow cross-correlation over a large redshift range, which will translate to a search over a large prior range for the cosmological parameters. In future, with the operation of the next generation GW detectors such as Laser Interferometer Space Antenna (LISA) (Amaro-Seoane et al. 2017), Einstein Telescope (Punturo et al. 2010), Cosmic Explorer (Reitze et al. 2019) and TianQin observatory (Luo et al. 2016), cross-correlation with Euclid galaxy survey will be very useful.

6 SIMULATED SAMPLES OF GW SOURCES AND GALAXIES

In this analysis, we do a Bayesian estimation of the GW source parameters using a nested sampler *dynesty* (Speagle 2020) which is a part of the *Bilby* package (Ashton et al. 2019) for a network of four detectors LIGO-Hanford, LIGO-Livingston, Virgo, and KAGRA. This is a very computationally heavy process and can be performed only for a few hundred sources within a decent time and available computing facility⁴. So, we will restrict our analysis only to the low

⁴ A single GW source parameter estimation (with six parameters) has taken < 10 hours to about 50 hours for heavier and lighter masses respectively.

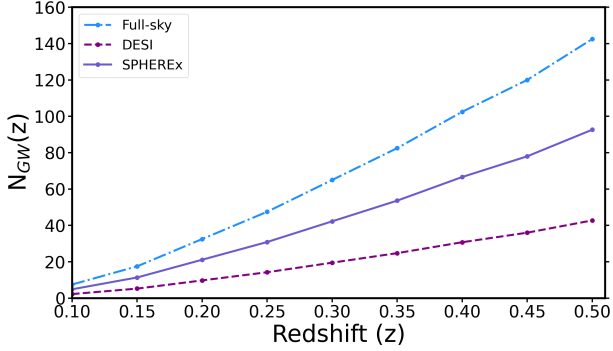


Figure 3. Number of GW sources in full-sky, in the DESI sky area, and in the SPHEREx sky area as a function of redshift z for the power-law time-delay parameter $t_d^{min} = 0.5$ Gyr, for 5 years of b =observation time with 50% duty cycle.

redshift ($z \leq 0.5$) to explore the cross-correlation study. This choice gives us a limited number of samples for which we can perform GW parameter estimation and propagate the uncertainties properly in the cross-correlation study to gauge its utility. As a result, we will be able to explore the synergy with only the mock catalog for low redshift BGS samples from a DESI survey and with the low-redshift galaxies from a SPHEREx survey. However, this choice is unlikely to make any major impact on the analysis, because the sources at higher redshift are going to have low matched-filter SNR than the nearby samples which will cause a larger luminosity distance error and also smaller a smaller value of k_{eff} . Both of these will make the estimation of the clustering redshift weak. The only positive aspect of going to high redshift is an increase in the total number of sources, which can make some improvement in the estimation of cosmological parameters. So, in a future analysis, we will use approximate-likelihood to consider GW sources up to high redshift to explore the synergy with DESI-ELG, Vera Rubin Observatory, and Roman Telescope. In this analysis, we will also not consider the spin parameters to reduce the computational time of the parameter estimation. However, this assumption is also not going to make any major impact on the cross-correlation study.

6.1 GW source catalog

To create our mock catalog of GW sources, we consider six parameters, namely the component masses of the two black holes m_1 and m_2 , the luminosity distance to the GW source d_l , the inclination angle $\theta_{jn} = \arccos(\hat{L} \cdot \hat{n})$ denote the angle between the angular momentum vector \hat{L} and the line of sight \hat{n} , and the sky localization parameters Right ascension (RA) and declination (DEC). Also, to generate a GW mock catalog, we need to consider a redshift distribution of the GW merger rates. We will briefly describe below all these aspects which are used to construct a mock GW catalog.

GW Merger rate: For making a mock catalog of GW sources, we need to assume a merger of GW sources as a function of redshift. We consider a GW merger rate model motivated by the [Madau & Dickinson \(2014\)](#) SFR and with power-law time-delay distribution with a minimum time-delay $t_d^{eff} = 0.5$ Gyr. The corresponding merger rate is shown in Fig. 1 in grey line. We consider a total observation time of

five years with a 50% duty cycle with a network of LVK detectors and perform an integral over the comoving volume with a redshift bin-width $\Delta z = 0.02$ and observation time to obtain the total number of samples $N_{GW}(z) = \int dt \int dz \frac{\mathcal{R}_{GW}(z)}{1+z} \frac{dV}{dz}$. The corresponding plot for the total number of sources is shown in Fig. 3 in a dashed-dotted line.

GW source mass distribution: In this analysis we assume a power-law distribution for the mass distribution of black holes. A power-law model for the BH mass distribution is used in LIGO data analysis, ([Abbott et al. 2019b, 2016a](#)). More recently, a power-law+peak model was found to be more suitable to the data with a peak around a mass of $30 - 40 M_\odot$. The presence of such a peak can provide additional cosmological information ([Farr et al. 2019; Mastrogiovanni et al. 2021a](#)) and also for heavier mass black holes, we can expect a better measurement of the luminosity distance than a lighter one. However, in this analysis, we have taken a pessimistic choice on the mass distribution. assuming it's a power-law distribution $M^{-\alpha}$ with a minimum mass $M_{min} = 5 M_\odot$ and a maximum mass $M_{max} = 50 M_\odot$ with a value of $\alpha = 2.35$. The lower mass limit in the mass is motivated by the lower mass gap. As for the upper limit, $m_{max} = 50 M_\odot$ is determined by the lower edge of the pair-instability gap in the BBH mass spectrum ([Abbott et al. 2016a; Farmer et al. 2019](#)). The mass distribution with a peak and appropriate modeling of that can help in improving the measurability of the cosmological parameters. To generate GW sources from the power-law distribution, we randomly generating the masses of the component black holes according to the power-law mass distribution using the acceptance-rejection method. This is performed for all the sources estimated $N_{GW}(z)$ for each redshift.

GW inclination angle: The inclination angle for the GW sources are considered randomly between $[0, \pi]$. For each redshift, we choose the number of θ_{jN} according to the value of $N_{GW}(z)$ obtained at each redshift.

GW sky position: The effect sky-area available for the cross-correlation study depends on the overlap between the GW sky-area (which can be considered to be all-sky), and the galaxy surveys (which is survey specific). In this analysis, we consider two surveys for exploring the cross-correlation study, namely DESI and SPHEREx. The DESI BGS galaxy sample is available over a sky-area of 14000 sq. deg, which corresponds to a sky-fraction $f_{sky} = 0.3$. For SPHEREx, in-principle the observation can be made over full-sky. But the effective sky-fraction f_{sky} considered in this analysis is 0.65. So, in our analysis, we randomly choose sky positions for the sources corresponding to the number accessible from DESI and SPHEREx. These are shown in Fig. 3 in dashed-line and solid-line for DESI and SPHEREx respectively.

Gravitational waveforms template: For the generation of the GW signal, we use the IMRPhenomPv2 ([Khan et al. 2019](#)) gravitational waveform, which is available with the Bilby package ([Ashton et al. 2019](#)). The IMRPhenomPv2 ([Khan et al. 2019](#)) waveform is generated in the frequency domain which is a single-precessing-spin waveform model. This is model is composed of a post-Newtonian approximation to the inspiral period of the waveform and a phenomenological approximation for the merger and ring-down phase ([Khan et al. 2019](#)).

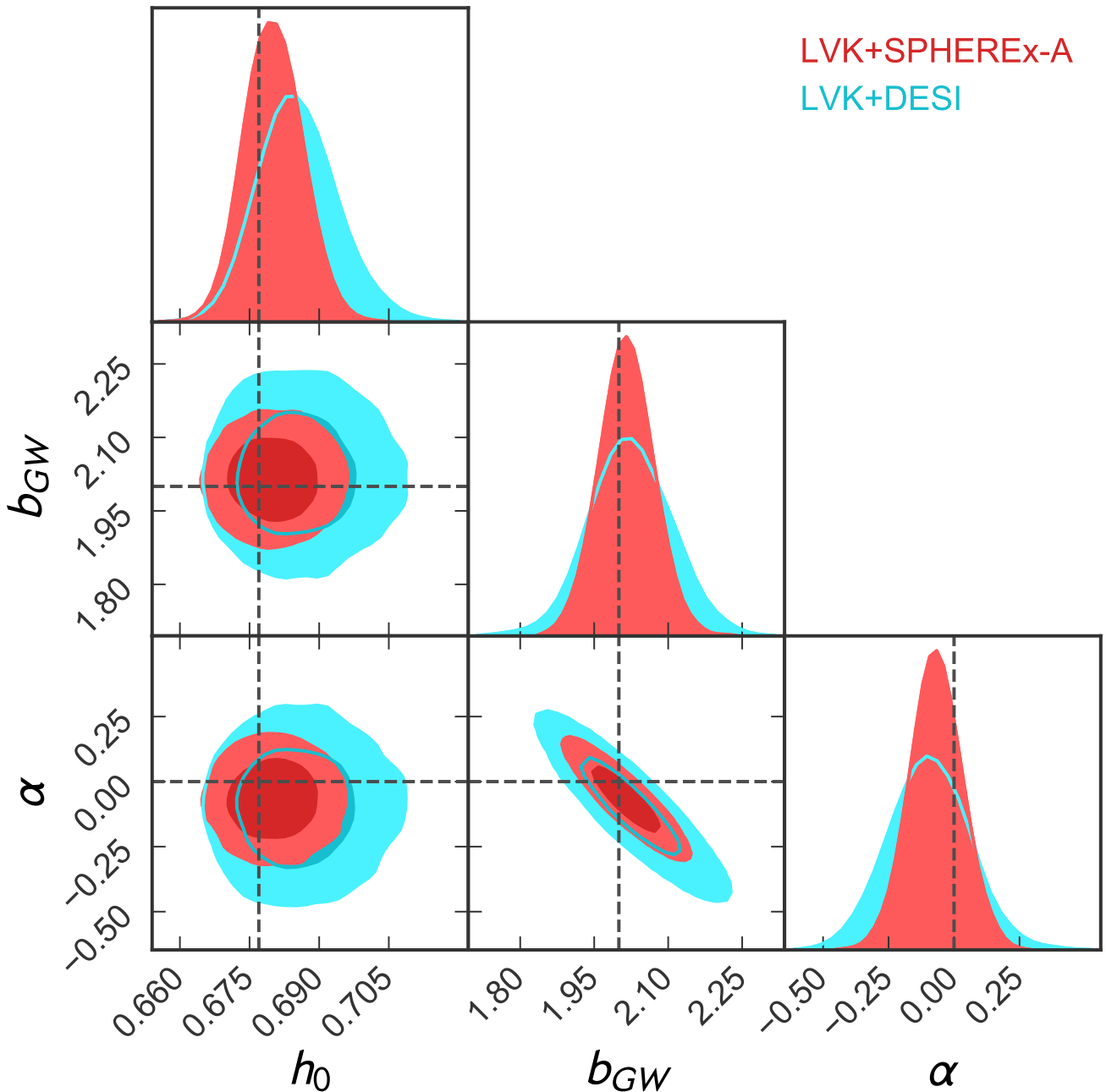


Figure 4. Forecast for the joint estimation of the Hubble constant $H_0 = 100h_0$ km/s/Mpc along with the GW bias parameter $b_{GW}(z) = b_{GW}(1+z)^\alpha$ from the GW sources detectable from the network of LVK detectors in combination with DESI (cyan) and SPHEREx-A (red). The injected values in the simulations are shown by the black dashed line.

6.2 Mock catalog of galaxy and GW sources

For the study of the cross-correlation between dark standard sirens and upcoming galaxy surveys, we generate mock catalogs of galaxies with the redshift window function and number density of objects specific to individual large-scale structure surveys namely DESI (Aghamousa et al. 2016), and SPHEREx-A (Doré et al. 2014; Dore et al. 2018b). The specifications for both these surveys are mentioned in Sec. 5.2. For both these mock galaxy catalogs we use the package `nbodykit` (Hand et al. 2018) including the effect of redshift space dis-

tortions. The maximum redshift is considered up to $z = 0.7$ which is deeper than the GW source distribution considered in this analysis. The galaxy catalogs for DESI and SPHEREx are considered with spectroscopic redshift uncertainties. The galaxy samples are produced with a linear model of galaxy bias in this study with $b_g = 1.6$ (Anderson et al. 2012; Desjacques et al. 2018; Alam et al. 2017a). As this analysis is restricted to low redshift, so we have neglected the contribution from weak lensing, which is primarily important for sources at high redshift (Holz & Wald 1998; Hirata et al.

2010; Mukherjee et al. 2020c). Though we do have not included Euclid in the mock catalog study, combining all the catalogs is going to be partly useful.

For the mock samples of GW sources, we obtain the GW spatial distribution from the same realization of the mock galaxy catalog with the population and source properties of the GW sources mentioned in Sec. 6.1. Due to the larger sky coverage of SPHEREx ($f_{sky} = 0.65$) than DESI ($f_{sky} = 0.3$), the total number of GW sources which will be overlapping with DESI sky area is going to be less than the total number of sources overlapping with SPHEREx. As a result, we consider we obtain the GW samples for the corresponding values of N_{GW} shown in Fig. 1. The overlap for this with GW merger rate with different spectroscopic galaxy surveys is shown in

$$\mathcal{P}(\Theta_c | \vec{\vartheta}_{GW}, \vec{d}_g) \propto \iint d\Theta_n dz \left[\prod_{i=1}^{N_{GW}} \mathcal{L}(\vec{\vartheta}_{GW} | P_{gg}^{ss}(\vec{k}, z), \Theta_n, \vec{d}_g(z)) \mathcal{P}(\vec{d}_g | P_{gg}^{ss}(\vec{k}, z)) \mathcal{P}(\{d_i^i\}_{GW} | z, \Theta_c, \{\theta^i, \phi^i\}_{GW}) \Pi(z) \right] \times \Pi(\Theta_n) \Pi(\Theta_c), \quad (9)$$

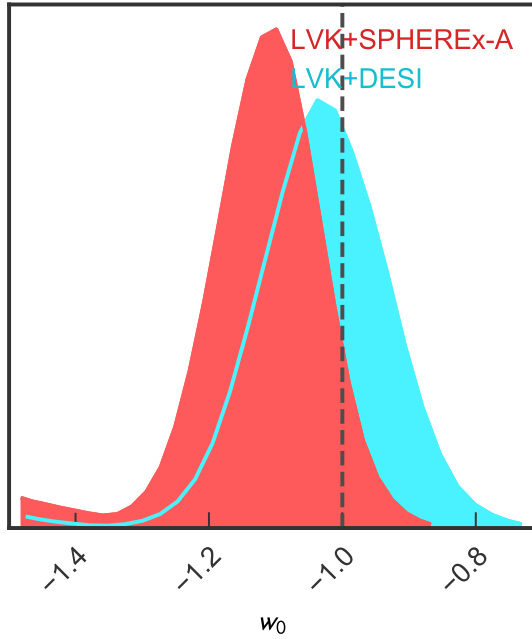


Figure 5. The posterior on the dark energy equation of state w_0 after marginalizing over the GW bias parameter and its redshift dependence is shown for LVK+DESI (cyan) and LVK+SPHEREx-A (red). The black dashed-line indicates the injected value $w_0 = -1$ used in the simulations.

where $\Pi(z)$, $\Pi(\Theta_n)$ and $\Pi(\Theta_c)$ denotes the prior on the redshift, nuisance parameters, and the cosmological parameters. $\mathcal{P}(\{d_i^i\}_{GW} | z, \Theta_c, \{\theta^i, \phi^i\}_{GW})$ denotes the posterior on the luminosity distance marginalised obtained from Bilby, $\mathcal{P}(\vec{d}_g | P_{gg}(\vec{k}, z))$ is the posterior of the galaxy density field related to the galaxy power spectrum $P_{gg}(\vec{k}, z)$. The likelihood in Eq. (9) $\mathcal{L}(\vec{\vartheta}_{GW} | P_{gg}(\vec{k}, z), \Theta_n, \vec{d}_g(z))$ can be written

Fig. 2 which shows the possible synergy expected between LVK+DESI and LVK+SPHEREx.

7 FORECAST FOR THE COSMOLOGICAL PARAMETERS

We explore the synergy between LVK+DESI and LVK+SPHEREx, by performing a joint Bayesian analysis following the framework developed in Mukherjee et al. (2021b,c). The posterior on the cosmological parameters can be inferred using the gravitational wave data vector $\vec{\vartheta}_{GW} \equiv \{d_i^i, \theta_{GW}^i, \phi_{GW}^i\}$ and the galaxy data vector $\vec{d}_g \equiv \{\delta_g(z_g^i, \theta_g^i, \phi_g^i)\}$ by

as (Mukherjee et al. 2021b)

$$\mathcal{L}(\vec{\vartheta}_{GW} | P_{gg}^{ss}(\vec{k}, z), \Theta_n, \vec{d}_g(z)) \propto \exp \left(- \frac{V_s}{4\pi^2} \int k^2 dk \int d\mu \times \mathbf{D}^\dagger(k, \mu, z) \mathbf{C}^{-1}(k, \mu, z) \mathbf{D}(k, \mu, z) \right), \quad (10)$$

where $\mathbf{D}(k, \mu, z) \equiv \hat{P}(\vec{k}, \Delta\Omega_{GW}) - b_g(k, z)b_{GW}(k, z)(1 + \beta_g \mu_k^2) P_m(k, z) e^{-\frac{k^2}{k_{eff}^2}}$, consists of the power spectrum estimated from data ($\hat{P}(\vec{k}, \Delta\Omega_{GW})$) and the model power spectrum ($b_g(k, z)b_{GW}(k, z)(1 + \beta_g \mu_k^2) P_m(k, z) e^{-\frac{k^2}{k_{eff}^2}}$). The value of effective Fourier modes up to which signal can be estimated is $1/k_{eff}^2 = \mu^2/(k_{max}^l)^2 + (1 - \mu^2)/(k_{max}^p)^2$, where the value of k_{max}^p and k_{max}^l are defined in Sec. 4. The covariance matrix considered in this analysis is $\mathbf{C}(k, \mu, z) \equiv 2(P_{gg}^{ss}(\vec{k}, z) + n_g(z)^{-1})(P_{GW}^{rr}(\vec{k}, z) + n_{GW}(z)^{-1})$ which is taken as diagonal in this analysis. At the large values of the Fourier modes k , the covariance matrix are also going to have off-diagonal terms. However, most of the those scales are not resolvable due to the sky localization error of 10 sq. deg or larger on the GW sources detectable from the LVK data analysis. So in this analysis, we ignore the off-diagonal terms. However, for the implementation of the technique on the data, we can consider the full survey-specific covariance matrix. For the DESI survey, we take the number density of BGS and ELGs according to the redshift distribution shown in Aghamousa et al. (2016). For SPHEREx, we only consider sources with the corresponding number distribution which are measurable with the redshift error $\sigma_z = 0.003(1+z)$ (Doré et al. 2014). We take priors as $\Pi(H_0) = \mathcal{U}[20, 150]$ km/s/Mpc, $\Pi w_0 = \mathcal{U}[-1.5, -0.3]$, $\Pi(b_{GW}) = \mathcal{U}[0, 6]$, and $\alpha = \mathcal{U}[-4, 4]$ for both LVK+DESI and LVK+SPHEREx analysis.

7.1 Measurement of the Hubble parameter and GW bias parameter

Using the cross-correlation technique, we investigate the measurability of the Hubble constant from the combination of LVK+DESI and LVK+SPHEREx missions. The sky-fraction of DESI is smaller than the sky-fraction available from SPHEREx. So, the number of GW sources overlapping with the DESI survey will be less than the SPHEREx survey. By combining the 5-years observational run of LVK, we show the forecast for the measurement of the Hubble constant, after marginalizing over the GW bias parameter b_{GW} and its redshift dependence α for the Lambda-Cold Dark Matter model of cosmology in Fig. 4 for LVK+DESI (in cyan) and LVK+SPHEREx (in red). The constraints are going to be about $\sim 2\%$ and $\sim 1.5\%$ measurement of the value of Hubble constant from LVK+DESI and LVK+SPHEREx respectively. The difference in the measurability is primarily driven by the smaller sky-fraction on DESI survey than SPHEREx. Also, as shown previously in Mukherjee et al. (2021b,c) this method will also be able to measure for the first time GW bias parameter $b_{GW}(z) = b_{GW}(1+z)^\alpha$ and shed light on its redshift dependence from both LVK+DESI and LVK+SPHEREx. With the availability of more GW sources, the error on the cosmological parameters will scale as $N_{GW}^{-1/2}$ (Mukherjee et al. 2021b,c). This method can take care of the peculiar velocity correction by implementing the method proposed by Mukherjee et al. (2021d) on DESI and SPHEREx data. When this method will be applied to the data, we will consider the covariance matrix estimated from simulations including the possible systematic specifics to these surveys.

7.2 Measurement of dark energy equation of state

The dark energy equation of state w_0 is another interesting quantity to understand the nature of cosmic acceleration. We have explored the measurability of this parameter from LVK+DESI and LVK+SPHEREx combinations after marginalizing over the GW bias parameters and show the corresponding 1-D marginalized posterior in Fig. 5. This shows that, we can make about a 10% measurement from LVK+DESI and a $\sim 8\%$ measurement from LVK+SPHEREx within the five years of observation. Joint estimation of the multiple cosmological parameters is possible, but the measurability will significantly degrade. As a result, to get interesting constraints within the first five years of LVK observation, it is appropriate to only get constraints on w_0 , and in the future with more sources, one can measure the parameters jointly. The difference in the peak value of the posterior distribution and the injected mean value is due to less number of sources, and with more sources, unbiased estimation is possible. With a longer observation run and more GW objects sources in lower luminosity distance, it will be possible to obtain better constraints on the cosmological parameters (Mukherjee et al. 2021b,c). For the third generation GW detectors such as Einstein Telescope (Punturo et al. 2010), and Cosmic Explorer (Reitze et al. 2019), with a large number of sources, this method will be able to reach much better precision in the measurement of w_0 . This method will also make it possible to measure the redshift dependence of the dark energy equation of state ($w(z) = w_z(z/(1+z))$) in a longer time scale with more GW sources (Mukherjee et al. 2021b).

8 CONCLUSION

In this paper, we explore the synergy between the ongoing GW detectors such as LIGO, Virgo, and KAGRA with the ongoing/upcoming spectroscopic surveys such as DESI, SPHEREx, and EUCLID to map the expansion history of the Universe from the dark standard sirens by inferring the clustering redshift of the GW sources using cross-correlation between GW sources and galaxies. One of the key requirements to infer the clustering redshift is the overlap in the redshift and sky-position of the GW sources with the spectroscopic galaxies. The redshift overlap between the detected GW sources and spectroscopic galaxy surveys depends on a few factors such as the merger rate of the GW sources, the horizon for a network of GW detectors, and the redshift space window function of spectroscopic surveys. We show in Fig. 2 that for GW mergers rates motivated by the Madau & Dickinson (2014) SFR for a time-delay $t_d^{eff} < 2$ Gyr, one would expect overlapping GW sources from the redshift range which are accessible from the combination of the BGS and ELG from DESI (Aghamousa et al. 2016) having a redshift error $\sigma_z = 0.001(1+z)$, SPHEREx-A and SPHEREx-B galaxy surveys with redshift errors $\sigma_z = 0.003(1+z)$ and $\sigma_z = 0.01(1+z)$ respectively (Doré et al. 2014), and Euclid (Blanchard et al. 2020) have $\sigma_z = 0.001(1+z)$. However, due to a detector horizon up to a redshift $z \sim 1.1$, sources beyond this redshift cannot contribute to the estimation of the cosmological parameters. For the implementation of the cross-correlation study and explore a large parameter space of the GW sources, we need to combine all different spectroscopic surveys mentioned above. In this work we focus only on DESI and SPHEREx-A, however some more improvements can also be made if we can combine Vera Rubin Observatory (Reid et al. 2009) and Roman Telescope (Green et al. 2012; Spergel et al. 2013; Dore et al. 2018a). We will explore the synergy with it in future work (under preparation).

To explore the measurability of the cosmological parameters using the cross-correlation technique, we consider simulated GW sources with IMRPhenomPv2 up to redshift $z = 0.5$ for five years of observation time with 50% duty cycle and perform a GW source parameter estimation in a Bayesian framework using the package Bilby (Ashton et al. 2019). We perform a Bayesian parameter estimation of the GW sources to correctly include degeneracy between different parameters and also for including the non-Gaussian posterior distributions of the source parameters. We restrict our analysis only to the low-redshift mock samples to reduce the computational cost in estimating the GW source parameters. Also, GW sources which are at high redshift, the error in the luminosity distance and sky localization are poor and hence will not make a significant difference in the measurability of the cosmological parameters. However, in a future work (under preparation) we will use approximate-likelihood to explore the synergy with Euclid, Vera Rubin Observatory, and Roman Telescope.

We find that both the combinations LVK+DESI and LVK+SPHEREx are very powerful in exploring the clustering redshift of the dark GW sources and can use it to measure the expansion history and GW bias parameter with both accuracy and precision. We find that LVK+DESI and LVK+SPHEREx can make about $\sim 2\%$ and $\sim 1.5\%$ measurement of the value of Hubble constant $H_0 = 67.7$ km/s/Mpc in five years of

observation of the LVK network of detectors with 50% duty cycle. This measurement is after marginalization of the selection effect which is captured by the GW bias parameters. In this setup, we will also be able to explore the redshift dependence of the GW bias parameter which captures how the GW sources trace the underlying dark matter distribution. Using the cross-correlation technique, we can also measure the value of dark energy equation of state w_0 (keeping H_0 and Ω_m) fixed with about 10% and 8% precision from LVK+DESI and LVK+SPHEREx respectively. The primary reason for the difference in the performance between LVK+DESI and LVK+SPHEREx is due to larger sky-fraction available to SPHEREx than DESI. In the future, with the operation of LIGO-India, a further improvement in the cross-correlation study is possible due to improvement in the sky-location error (Unnikrishnan 2013). To achieve, accurate and precise measurement of expansion history, it is also important to mitigate the possible systematics which can arise from the GW waveform modeling and instrument calibration (Sun et al. 2020; Bhattacharjee et al. 2020; Vitale et al. 2021). Though in this work, we mainly explore the synergy with the galaxy surveys and LVK detectors to explore cosmology, in a future analysis impact of waveform systematics and instrument calibration will be explored. In addition to the dark sirens, detection of bright *standard sirens* (Chen et al. 2018; Feeney et al. 2019; Mukherjee et al. 2020a) can provide additional improvement in measuring the Hubble constant, dark energy equation of state.

In summary, this study shows the possible synergy between the GW detectors and galaxy surveys in exploring cosmology. This multi-messenger avenue will shed light not only in resolving the tension in the value of Hubble constant between the low redshift probes (Efstathiou 2014; Riess et al. 2019; Riess 2019; Wong et al. 2020; Freedman et al. 2019, 2020; Soltis et al. 2021) and the high redshift probes (Spergel et al. 2003, 2007; Komatsu et al. 2011; Planck collaboration 2014; Ade et al. 2016; Alam et al. 2017b; Aghanim et al. 2018; Verde et al. 2019; Alam et al. 2021; Aiola et al. 2020; Di Valentino et al. 2021), but will also provide an independent measurement of the dark equation of state which can bring a better understanding of its nature and its interaction with the tensor sector. This synergistic study will provide the first measurement of the GW bias parameter and its redshift dependence and will shed light on its connection with the dark matter distribution in the Universe. Finally, the cross-correlation technique between the GW sector and galaxies will be able to test the general theory of relativity which is currently not feasible from only the electromagnetic observations (Mukherjee et al. 2020b,c, 2021c).

ACKNOWLEDGEMENTS

The authors are grateful to Archisman Ghosh for reviewing the manuscript as a part of LVK publication and presentation policy. SM acknowledges useful inputs from Martin Hendry on this work. A part of this work is carried out under the Master's program at the University of Amsterdam. This work is part of the Delta ITP consortium, a program of the Netherlands Organisation for Scientific Research (NWO) that is funded by the Dutch Ministry of Education, Culture, and Science (OCW). This analysis is car-

ried out at the Infinity cluster, the Horizon cluster hosted by Institut d'Astrophysique de Paris, and the Lisa cluster hosted by the University of Amsterdam. We thank Stephane Rouberol for smoothly running the Infinity cluster and the Horizon cluster. We acknowledge the use of following packages in this work: **Astropy** (Astropy Collaboration et al. 2013, 2018), **Bilby** (Ashton et al. 2019), **DYNesty** (Speagle 2020), **emcee: The MCMC Hammer** (Foreman-Mackey et al. 2013), **Giant-Triangle-Confusogram** (Bocquet & Carter 2016), **IPython** (Pérez & Granger 2007), **Matplotlib** (Hunter 2007), **nboddykit** (Hand et al. 2018), **NumPy** (van der Walt et al. 2011), and **SciPy** (Jones et al. 01). The authors thank the SPHEREx science team for providing the galaxy distribution. The authors would like to thank the LIGO/Virgo scientific collaboration for providing the noise curves. LIGO is funded by the U.S. National Science Foundation. Virgo is funded by the French Centre National de Recherche Scientifique (CNRS), the Italian Istituto Nazionale della Fisica Nucleare (INFN), and the Dutch Nikhef, with contributions by Polish and Hungarian institutes. This material is based upon work supported by NSF's LIGO Laboratory which is a major facility fully funded by the National Science Foundation.

DATA AVAILABILITY

The data underlying this article will be shared at request to the corresponding author.

REFERENCES

- Aasi J., et al., 2015a, *Class. Quant. Grav.*, 32, 074001
Aasi J., et al., 2015b, *Classical and Quantum Gravity*, 32, 074001
Abbott B., et al., 2016a, *Physical Review X*, 6
Abbott B. P., et al., 2016b, *Phys. Rev. D*, 93, 112004
Abbott B. P., et al., 2016c, *Phys. Rev. Lett.*, 116, 061102
Abbott B. P., et al., 2016d, *The Astrophysical Journal*, 818, L22
Abbott B. P., et al., 2017a, *Phys. Rev. Lett.*, 119, 161101
Abbott B., et al., 2017b, *Astrophys. J. Lett.*, 848, L12
Abbott B. P., et al., 2018, *Living Rev. Rel.*, 21, 3
Abbott B., et al., 2019a, arXiv:1908.06060
Abbott B., et al., 2019b, *Physical Review X*, 9
Abbott R., et al., 2020a, arXiv preprint arXiv:2010.14533
Abbott R., et al., 2020b, *Phys. Rev. Lett.*, 125, 101102
Abbott B. P., et al., 2020c, *The Astrophysical Journal*, 892, L3
Abbott R., et al., 2020d, *Astrophys. J.*, 896, L44
Abbott R., et al., 2021, *Physical Review X*, 11
Acernese F., et al., 2014, *Classical and Quantum Gravity*, 32, 024001
Acernese F., et al., 2019, *Phys. Rev. Lett.*, 123, 231108
Ade P., et al., 2016, *Astron. Astrophys.*, 594, A13
Aghamousa A., et al., 2016, arXiv preprint arXiv:1611.00036
Aghanim N., et al., 2018, arXiv:1807.06209
Aiola S., et al., 2020, *JCAP*, 12, 047
Akutsu T., et al., 2019a, *Nat. Astron.*, 3, 35
Akutsu T., et al., 2019b, *Nature Astron.*, 3, 35
Akutsu T., et al., 2020, arXiv:2005.05574
Alam S., et al., 2017a, *MNRAS*, 470, 2617
Alam S., et al., 2017b, *Mon. Not. Roy. Astron. Soc.*, 470, 2617
Alam S., et al., 2021, *Phys. Rev. D*, 103, 083533
Amaro-Seoane P., et al., 2017, arXiv e-prints, p. arXiv:1702.00786
Anderson L., et al., 2012, *MNRAS*, 427, 3435

- Antonini F., Rasio F. A., 2016, *The Astrophysical Journal*, 831, 187
- Arabsalmani M., Sahni V., Saini T. D., 2013, *Phys. Rev. D*, 87, 083001
- Ashton G., et al., 2019, *The Astrophysical Journal Supplement Series*, 241, 27
- Astropy Collaboration et al., 2013, *A&A*, 558, A33
- Astropy Collaboration et al., 2018, *AJ*, 156, 123
- Banerjee S., Baumgardt H., Kroupa P., 2010, *MNRAS*, 402, 371
- Bera S., Rana D., More S., Bose S., 2020, *Astrophys. J.*, 902, 79
- Bhattacharjee D., Lecoche Y., Karki S., Betziewer J., Bossilkov V., Kandhasamy S., Payne E., Savage R., 2020, arXiv:2006.00130
- Blanchard A., et al., 2020, *Astron. Astrophys.*, 642, A191
- Bocquet S., Carter F. W., 2016, *The Journal of Open Source Software*, 1
- Calore F., Cuoco A., Regimbau T., Sachdev S., Serpico P. D., 2020, *Physical Review Research*, 2
- Cao L., Lu Y., Zhao Y., 2018, *MNRAS*, 474, 4997
- Chan M. L., 2018, PhD thesis, Glasgow U.
- Chen H.-Y., Fishbach M., Holz D. E., 2018, *Nature*, 562, 545
- Chen H.-Y., Haster C.-J., Vitale S., Farr W. M., Isi M., 2020, arXiv:2009.14057
- Coleman Miller M., Hamilton D. P., 2002, *Monthly Notices of the Royal Astronomical Society*, 330, 232–240
- Dalal N., Holz D. E., Hughes S. A., Jain B., 2006, *Phys. Rev. D*, 74, 063006
- Dálya G., et al., 2018, *Mon. Not. Roy. Astron. Soc.*, 479, 2374
- Davis M., Peebles P. J. E., 1977, *ApJS*, 34, 425
- Davis M., Peebles P. J. E., 1983, *ApJ*, 267, 465
- Dawson K. S., et al., 2013, *AJ*, 145, 10
- Del Pozzo W., 2012, *Phys. Rev. D*, 86, 043011
- Desjacques V., Jeong D., Schmidt F., 2018, *Phys. Rept.*, 733, 1
- Di Valentino E., et al., 2021, *Class. Quant. Grav.*, 38, 153001
- Dominik M., Belczynski K., Fryer C., Holz D. E., Berti E., Bulik T., Mandel I., O’Shaughnessy R., 2012, *ApJ*, 759, 52
- Dominik M., et al., 2015, *Astrophys. J.*, 806, 263
- Doré O., et al., 2014, arXiv preprint arXiv:1412.4872
- Dore O., et al., 2018b, arXiv
- Dore O., et al., 2018a, preprint (arXiv:1804.03628)
- Efstathiou G., 2014, *Mon. Not. Roy. Astron. Soc.*, 440, 1138
- Eisenstein D. J., Hu W., 1997, *Astrophys. J.*, 511, 5
- Eisenstein D. J., Hu W., 1998, *Astrophys. J.*, 496, 605
- Elbert O. D., Bullock J. S., Kaplinghat M., 2018, *Mon. Not. Roy. Astron. Soc.*, 473, 1186
- Eldridge J. J., Stanway E. R., Tang P. N., 2019, *Mon. Not. Roy. Astron. Soc.*, 482, 870
- Farmer R., Renzo M., de Mink S. E., Marchant P., Justham S., 2019, *The Astrophysical Journal*, 887, 53
- Farr W. M., Fishbach M., Ye J., Holz D., 2019, *Astrophys. J. Lett.*, 883, L42
- Feeney S. M., Peiris H. V., Williamson A. R., Nisanke S. M., Mortlock D. J., Alsing J., Scolnic D., 2019, *Phys. Rev. Lett.*, 122, 061105
- Finke A., Foffa S., Iacovelli F., Maggiore M., Mancarella M., 2021, arXiv:2101.12660
- Fishbach M., et al., 2019, *Astrophys. J. Lett.*, 871, L13
- Foreman-Mackey D., Hogg D. W., Lang D., Goodman J., 2013, *PASP*, 125, 306
- Foucart F., Hinderer T., Nisanke S., 2018, *Phys. Rev. D*, 98, 081501
- Freedman W. L., et al., 2019, arXiv:1907.05922
- Freedman W. L., et al., 2020, arXiv:2002.01550
- Gayathri V., et al., 2021, *Astrophys. J. Lett.*, 908, L34
- Graham M. J., et al., 2020, *Phys. Rev. Lett.*, 124, 251102
- Gray R., et al., 2020, *Phys. Rev. D*, 101, 122001
- Green J., et al., 2012, arXiv e-prints, p. arXiv:1208.4012
- Grover K., Fairhurst S., Farr B. F., Mandel I., Rodriguez C., Sidery T., Vecchio A., 2014, *Phys. Rev. D*, 89, 042004
- Gultekin K., Miller M. C., Hamilton D. P., 2004, *The Astrophysical Journal*, 616, 221–230
- Hamilton A. J. S., 1998, *The Evolving Universe*, p. 185–275
- Hand N., Feng Y., Beutler F., Li Y., Modi C., Seljak U., Slepian Z., 2018, *Astron. J.*, 156, 160
- Hirata C. M., Holz D. E., Cutler C., 2010, *Phys. Rev. D*, 81, 124046
- Holz D. E., Hughes S. A., 2005, *ApJ*, 629, 15
- Holz D. E., Wald R. M., 1998, *Phys. Rev. D*, 58, 063501
- Howell E. J., et al., 2018, *Mon. Not. Roy. Astron. Soc.*, 474, 4385
- Howlett C., Davis T. M., 2020, *Mon. Not. Roy. Astron. Soc.*, 492, 3803
- Hunter J. D., 2007, *Computing In Science & Engineering*, 9, 90
- Jones E., Oliphant T., Peterson P., et al., 2001–, SciPy: Open source scientific tools for Python, <http://www.scipy.org/>
- Kaiser N., 1987, *MNRAS*, 227, 1
- Kasliwal M., et al., 2017, *Science*, 358, 1559
- Khan S., Chatziioannou K., Hannam M., Ohme F., 2019, *Physical Review D*, 100
- Komatsu E., et al., 2011, *ApJS*, 192, 18
- LSST Science Collaboration et al., 2009, preprint, (arXiv:0912.0201)
- Lamberts A., Garrison-Kimmel S., Clausen D. R., Hopkins P. F., 2016, *Mon. Not. Roy. Astron. Soc.*, 463, L31
- Landy S. D., Szalay A. S., 1993, *ApJ*, 412, 64
- Laureijs R., et al., 2011, arXiv preprint arXiv:1110.3193
- Luo J., et al., 2016, *Class. Quant. Grav.*, 33, 035010
- MacLeod C. L., Hogan C. J., 2008, *Phys. Rev. D*, 77, 043512
- Madau P., Dickinson M., 2014, *Annual Review of Astronomy and Astrophysics*, 52, 415–486
- Mandel I., de Mink S. E., 2016, *MNRAS*, 458, 2634
- Mastrogiovanni S., et al., 2021a, arXiv:2103.14663
- Mastrogiovanni S., Haegel L., Karathanasis C., Hernandez I. M. n., Steer D. A., 2021b, *JCAP*, 02, 043
- McClelland J., Silk J., 1977a, *ApJ*, 216, 665
- McClelland J., Silk J., 1977b, *ApJ*, 217, 331
- McKernan B., et al., 2019, *Astrophys. J. Lett.*, 884, L50
- Menard B., Scranton R., Schmidt S., Morrison C., Jeong D., Budavari T., Rahman M., 2013, arXiv:1303.4722
- Messenger C., Read J., 2012, *Phys. Rev. Lett.*, 108, 091101
- Mukherjee S., Silk J., 2019, *Monthly Notices of the Royal Astronomical Society*
- Mukherjee S., Silk J., 2021, arXiv:2105.11139
- Mukherjee S., Wandelt B. D., 2018, arXiv:1808.06615
- Mukherjee S., et al., 2020a, arXiv:2009.14199
- Mukherjee S., Wandelt B. D., Silk J., 2020b, *Phys. Rev. D*, 101, 103509
- Mukherjee S., Wandelt B. D., Silk J., 2020c, *Mon. Not. Roy. Astron. Soc.*, 494, 1956
- Mukherjee S., Broadhurst T., Diego J. M., Silk J., Smoot G. F., 2021a, Impact of astrophysical binary coalescence timescales on the rate of lensed gravitational wave events (arXiv:2106.00392)
- Mukherjee S., Wandelt B. D., Nisanke S. M., Silvestri A., 2021b, *Physical Review D*, 103
- Mukherjee S., Wandelt B. D., Silk J., 2021c, *Mon. Not. Roy. Astron. Soc.*, 502, 1136
- Mukherjee S., Lavaux G., Bouchet F. R., Jasche J., Wandelt B. D., Nisanke S. M., Leclercq F., Hotokezaka K., 2021d, *Astron. Astrophys.*, 646, A65
- Nair R., Bose S., Saini T. D., 2018, *Phys. Rev. D*, 98, 023502
- Newman J. A., 2008, *Astrophys. J.*, 684, 88
- Nicolaou C., Lahav O., Lemos P., Hartley W., Braden J., 2020, *Mon. Not. Roy. Astron. Soc.*, 495, 90
- Nisanke S., Holz D. E., Hughes S. A., Dalal N., Sievers J. L., 2010, *ApJ*, 725, 496

- O'Shaughnessy R., Kalogera V., Belczynski K., 2010, *ApJ*, **716**, 615
- Oguri M., 2016, *Phys. Rev. D*, **93**, 083511
- Peebles P. J. E., Groth E. J., 1975, *ApJ*, **196**, 1
- Pérez F., Granger B. E., 2007, *Computing in Science and Engineering*, **9**, 21
- Perlmutter S., et al., 1999, *Astrophys. J.*, **517**, 565
- Planck collaboration 2014, *Astron. Astrophys.*, **571**, A16
- Punturo M., et al., 2010, *Class. Quant. Grav.*, **27**, 194002
- Reid M. J., Braatz J. A., Condon J. J., Greenhill L. J., Henkel C., Lo K. Y., 2009, *ApJ*, **695**, 287
- Reitze D., et al., 2019, *Bull. Am. Astron. Soc.*, **51**, 035
- Riess A. G., 2019, *Nature Rev. Phys.*, **2**, 10
- Riess A. G., Casertano S., Yuan W., Macri L. M., Scolnic D., 2019, *Astrophys. J.*, **876**, 85
- Rodriguez C. L., Zevin M., Amaro-Seoane P., Chatterjee S., Kremer K., Rasio F. A., Ye C. S., 2019, *Phys. Rev. D*, **100**, 043027
- Santoliquido F., Mapelli M., Giacobbo N., Bouffanais Y., Artale M. C., 2021, *Mon. Not. Roy. Astron. Soc.*, **502**, 4877
- Scelfo G., Bellomo N., Raccanelli A., Matarrese S., Verde L., 2018, *JCAP*, **09**, 039
- Scelfo G., Boco L., Lapi A., Viel M., 2020, *JCAP*, **10**, 045
- Schmidt S., Menard B., Scranton R., Morrison C., McBride C., 2013, *Mon. Not. Roy. Astron. Soc.*, **431**, 3307
- Schutz B. F., 1986, *Nature*, **323**, 310
- Schutz B. F., 2011, *Classical and Quantum Gravity*, **28**, 125023
- Soares-Santos M., et al., 2019, *Astrophys. J. Lett.*, **876**, L7
- Soltis J., Casertano S., Riess A. G., 2021, *Astrophys. J. Lett.*, **908**, L5
- Speagle J. S., 2020, *MNRAS*, **493**, 3132
- Spergel D., et al., 2003, *Astrophys. J. Suppl.*, **148**, 175
- Spergel D., et al., 2007, *Astrophys. J. Suppl.*, **170**, 377
- Spergel D., et al., 2013, arXiv e-prints, p. [arXiv:1305.5425](https://arxiv.org/abs/1305.5425)
- Sun L., et al., 2020, arXiv:2005.02531
- Tagawa H., Kocsis B., Haiman Z., Bartos I., Omukai K., Samsing J., 2021, *Astrophys. J. Lett.*, **907**, L20
- Unnikrishnan C., 2013, *Int. J. Mod. Phys. D*, **22**, 1341010
- Verde L., Treu T., Riess A., 2019, in Tensions between the Early and the Late Universe. ([arXiv:1907.10625](https://arxiv.org/abs/1907.10625)), [doi:10.1038/s41550-019-0902-0](https://doi.org/10.1038/s41550-019-0902-0)
- Vijaykumar A., Saketh M. V. S., Kumar S., Ajith P., Choudhury T. R., 2020, Probing the large scale structure using gravitational-wave observations of binary black holes ([arXiv:2005.01111](https://arxiv.org/abs/2005.01111))
- Vitale S., Haster C.-J., Sun L., Farr B., Goetz E., Kissel J., Cahillane C., 2021, *Phys. Rev. D*, **103**, 063016
- Wong K. C., et al., 2020, *Mon. Not. Roy. Astron. Soc.*, **498**, 1420
- Yang Y., et al., 2019, *Phys. Rev. Lett.*, **123**, 181101
- du Buisson L., et al., 2020, *Mon. Not. Roy. Astron. Soc.*, **499**, 5941
- van der Walt S., Colbert S. C., Varoquaux G., 2011, *Computing in Science and Engineering*, **13**, 22